

## Chapter 3

# Properties of Elliptical Galaxies

In the last 20 years our notions about elliptical galaxies have changed radically; these galaxies are much more complex than they seemed at first.

### 3.1 Folklore & Mythology

Traditionally, elliptical galaxies were seen as simple monolithic systems. Their overall luminosity profiles appeared to follow de Vaucouleurs' (1948) law, while their central regions fit the constant-density cores of King (1966) models. Elliptical galaxies were assumed to be oblate spheroids, flattened by rotation. The stars within them were thought to comprise a single, ancient population like the bulge and halo populations of our galaxy; gas and dust were thought to be absent. Finally, elliptical galaxies were considered to be relaxed and dynamically quiescent.

At one level or another, *all* of the above are incorrect.

### 3.2 Luminosity Profiles

Elliptical galaxies (and the bulges of disk galaxies) are often fit to de Vaucouleurs' (1948) law, also known as the “ $R^{1/4}$  law”:

$$I(R) = I_0 \exp(-kR^{1/4}), \quad (3.1)$$

where  $I(R)$  is the radial intensity profile,  $I_0$  is the central surface brightness, and  $k$  is a constant. This *empirical* rule has no real theoretical justification – as G. de Vaucouleurs said, this law is really just “a good French curve”. Certain elliptical galaxies, such as NGC 1700 (Capaccioli, Piotto, & Rampazzo 1988), fit (3.1) extremely well over a range of nearly 10 magnitudes in surface brightness, but other bona fide ellipticals do not. Stellar systems subjected to rapidly changing gravitational fields may develop profiles which resemble (3.1), but this depends on the kind of initial conditions used in the experiment.

Because the measurement of  $I_0$  depends on seeing conditions, it's often more convenient to use the equivalent form

$$I(R) = I_e \exp(-7.67((R/R_e)^{1/4} - 1)), \quad (3.2)$$

where  $I_e$  is the surface brightness of the isophote containing *half* the total light and  $R_e$  is the *effective radius* of that isophote.

### 3.2.1 Central profiles

In photographic photometry at arc-second resolution, elliptical galaxies appear to have luminosity profiles which flatten off as the projected radius  $R \rightarrow 0$  (King 1978). Such luminosity profiles can be fit by a modified Hubble law:

$$I(R) = \frac{I_0}{1 + (R/R_c)^2}, \quad (3.3)$$

where  $I_0$  is the central surface brightness and  $R_c$  is the *core radius*. The corresponding luminosity density profile is

$$j(r) = \frac{j_0}{[1 + (r/R_c)^2]^{3/2}} \quad (3.4)$$

where  $j_0 = I_0/2R_c$  is the central luminosity density; this profile flattens out at small radii, so  $dj/dr \rightarrow 0$  as  $r \rightarrow 0$ .

However, Schweizer (1979) showed that the observations may also be fit by a de Vaucouleurs law convolved with a point-spread function; as (3.1) continues rising as  $R \rightarrow 0$ , the *reality* of the cores seen in the photometry was called into question. Ground-based CCD photometry (Lauer 1985b, Kormendy 1987) showed that the apparent cores in some nearby elliptical galaxies are not entirely artifacts of seeing. These galaxies have luminosity profiles which ‘break’ away from a steep slope to a more shallow one; the *break* at least is real. But within this break radius the seeing-deconvolved luminosity profile continues to slowly rise, contradicting (3.3).

HST photometry shows that cores of *constant* surface density are a myth (Ferrarese et al. 1994, Lauer et al. 1995). In some galaxies the deconvolved luminosity profile rises steeply all the way to the pre-repair resolution limit of about 0.1 arcsec; these Lauer et al. call ‘power-law’ galaxies since their inner luminosity profiles fit power-laws with logarithmic slopes  $< -0.5$ . In others the profile rises steeply to a break, and then more slowly further in; these they call ‘core’ galaxies. This is a bad terminology since *none* of these galaxies actually have constant-density cores; inside of the break, luminosity profiles rise gradually, but the slope is never zero.

The implications of such profiles can be illustrated by a simple model. Suppose the luminosity density follows a power-law:

$$j(r) = j_*(r/r_*)^\gamma \quad (3.5)$$

where  $\gamma < -1$ . The corresponding surface-brightness profile is

$$I(R) = \int_{-\infty}^{\infty} dz j(\sqrt{R^2 + z^2}) = I_*(R/r_*)^{(\gamma+1)}, \quad (3.6)$$

where  $I_* = [\sqrt{\pi}\Gamma(-\frac{\gamma+1}{2})/\Gamma(-\frac{\gamma}{2})]j_*r_*$  is the surface brightness at  $R = r_*$ . Thus  $I(R)$  is also a power-law, with a slope one unit shallower than the slope of  $j(r)$ . Galaxies with steep power-law profiles typically have  $\gamma + 1 \simeq -1$ , implying 3-D luminosity profiles with slopes of  $\gamma \simeq -2$ , while galaxies with well-resolved breaks typically have  $\gamma + 1 \simeq -0.3$ , implying  $\gamma \simeq -1.3$ . In the limiting case  $\gamma = -1$  the integral in (3.6) won’t converge unless  $j(r)$  is truncated at large  $r$ ; the resulting  $I(R)$  profile diverges only logarithmically as  $R \rightarrow 0$ .

Projections of some more realistic galaxy models are shown in Fig. 3.1. These are based on the ‘gamma profile’ (Dehnen 1993, Tremaine et al. 1994), which has the form

$$j(r) = \frac{3-\gamma}{4\pi} \frac{aL}{r^\gamma(a+r)^{4-\gamma}}, \quad (3.7)$$

where  $a$  is a scale radius and  $\gamma$  parametrizes the slope of the central cusp. At radii  $r \ll a$  the luminosity density  $j(r) \propto r^{-\gamma}$ , while at  $r \gg a$  it is  $j(r) \propto r^{-4}$ . The images shown here were produced by flattening 3-D profiles of the form (3.7) by 20% along the vertical axis, and integrating the result along the line of sight. The model in (a) and (b) has a constant-density core ( $\gamma = 0$ ), while the one in (c) and (d) has a shallow cusp ( $\gamma = 1$ ). Note that these models *appear* very similar in projection, although the latter is slightly brighter at the center. In contrast, the model in (e) and (f), which has a steep cusp ( $\gamma = 2$ ), can easily be distinguished from the other two; even the grey-scale image reveals a sharp central peak in the surface brightness.

### 3.3 Shapes

Projected ellipticity  $\varepsilon \equiv 1 - b/a$  is determined by measuring the major and minor axes  $a$  and  $b$  of a chosen isophote. Results range from  $\varepsilon = 0$  to 0.7, but not flatter (Schechter 1987). While the ellipticity of any individual galaxy depends on unknown viewing angle as well as intrinsic shape, some information on the intrinsic shapes of E galaxies may be gleaned from a statistical analysis of the distribution of  $\varepsilon$  for a large sample. Models based on oblate shapes predict that large samples of randomly-oriented ellipticals should include a substantial number of galaxies with nearly circular isophotes ( $\varepsilon \simeq 0$ ). In fact, round galaxies are relatively rare compared to galaxies with  $\varepsilon \simeq 0.2$  (MB98, Fig. 4.33); this suggests that most elliptical galaxies are not oblate spheroids.

The ellipticity and position angle of a typical E galaxy depend on the surface brightness used to define the isophote measured; ellipticities reported in galaxy classification schemes generally represent some sort of subjective average over a range of surface brightnesses. A wide range of ellipticity profiles are represented in the data (Jedrzejewski 1987). Systematic changes in position angle – also known as isophotal twists – are common. It’s unlikely that any *intrinsically* twisted galaxy could be dynamically stable, and galaxies with nested oblate surfaces of constant stellar density will never exhibit twists in projection. But photometric twists like those observed can result if the surfaces of constant stellar density are triaxial ellipsoids with axial ratios varying with radius, as illustrated in Fig. 3.2. Thus isophotal twists are generally interpreted as evidence for *triaxiality* (Kormendy 1982).

#### 3.3.1 Non-elliptical isophotes

High signal-to-noise CCD images of elliptical galaxies show that many have non-elliptical isophotes (Carter 1979, 1987; Lauer 1985a; Jedrzejewski 1987; Bender, Dobereiner, & Mollenhoff 1988; Kormendy & Djorgovski 1989, hereafter KD89). Departures from a perfectly elliptical form typically have amplitudes of a few percent, and most galaxies are either *boxy* or *pointed*. Two related methods are used to measure isophote shapes. Both assume that one has already fit an ellipse to the isophote in question, and thereby determined its center, ellipticity, and position angle. Let  $a$  be the semi-major axis of this best-fitting ellipse.

**Isophote fitting** (Carter 1979). As a function of the angle  $\theta$  measured with respect to the major axis, the difference in radius between the actual isophote and the best-fit ellipse is fit to

$$\delta R(\theta) = \sum_{j=3} a_j \cos(j\theta) + b_j \sin(j\theta). \quad (3.8)$$

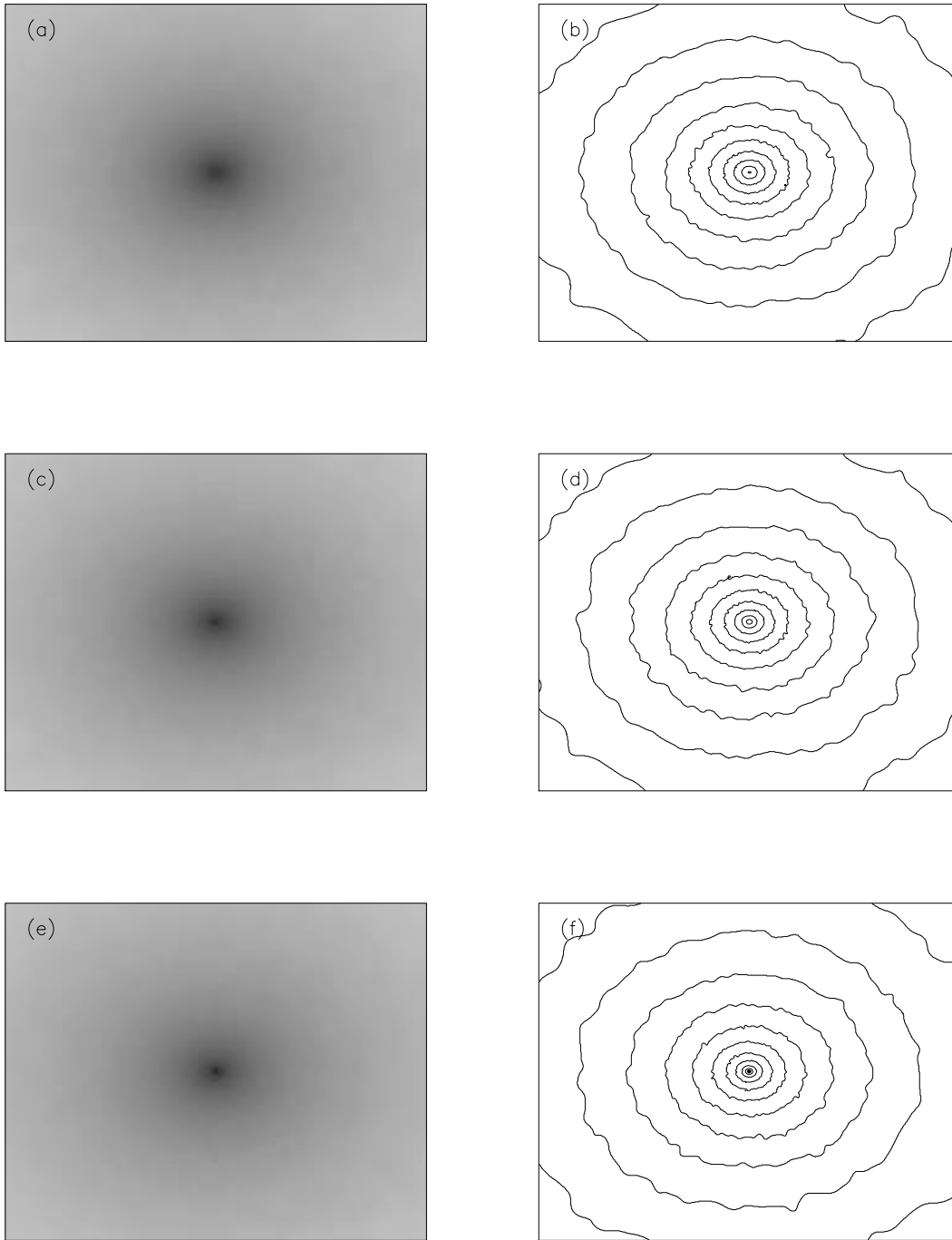


Figure 3.1: Simulated images of E2 galaxies. (a) Projection of 3-D luminosity profile  $j(r) \propto (a + r)^{-4}$ . (b) Isophotes of (a). (c) Projection of  $j(r) \propto r^{-1}(a + r)^{-3}$ . (d) Isophotes of (c). (e) Projection of  $j(r) \propto r^{-2}(a + r)^{-2}$ . (f) Isophotes of (e). Contours are separated by one magnitude. All luminosity profiles  $j(r)$  are scaled to have the same 3-D half-light radius; their *projected* half-light radii vary by only a few percent.

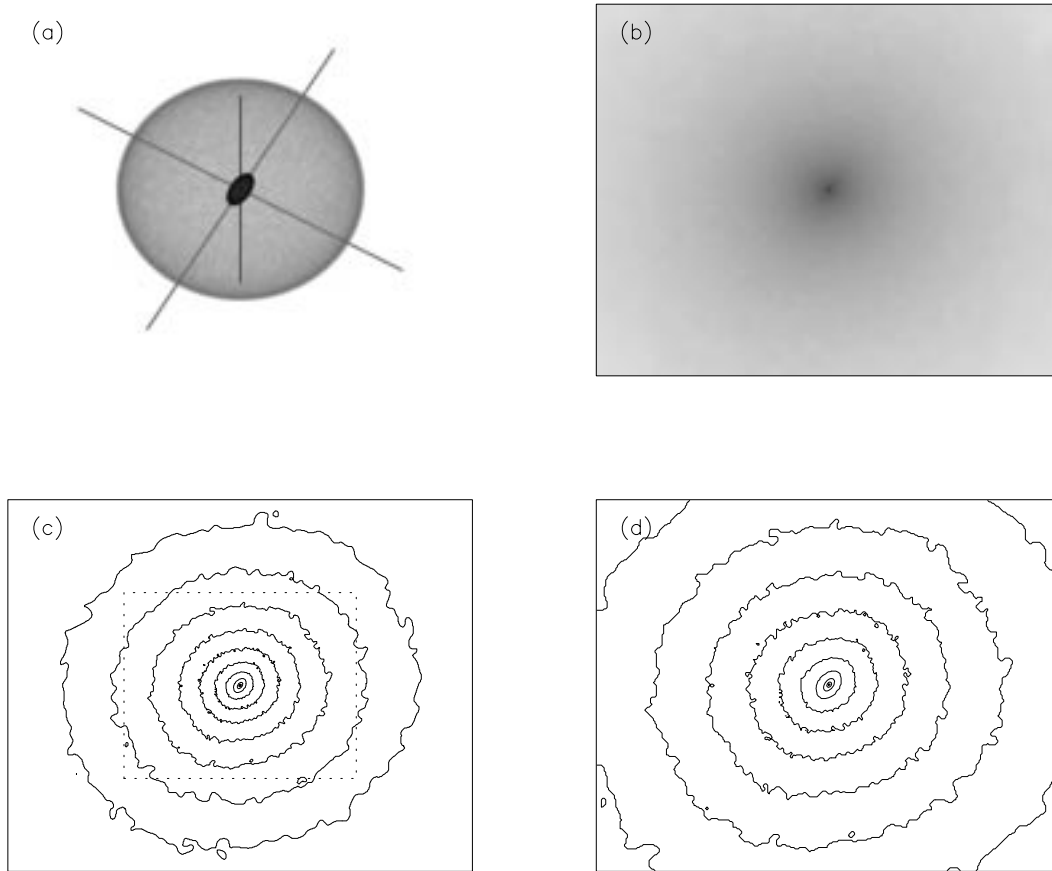


Figure 3.2: Projection of a triaxial galaxy model. (a) Surfaces of constant density. The outer surface is oblate, with axial ratios  $x : y : z = 1 : 1 : 0.46$ ; the inner surface is triaxial, with axial ratios  $x : y : z = 1 : 0.5 : 0.25$ . (b) Half-tone view of the projected surface brightness. (c) Isophotes of (b). (d) Isophotes of central region, outlined by dotted box in (c); note the twist in isophotal axes.

**Surface-brightness fitting** (Lauer 1985b). Again as a function of  $\theta$ , the surface brightness along the best-fit ellipse is fit to

$$I(\theta) = A + \sum_{j=3} A_j \cos(j\theta) + B_j \sin(j\theta). \quad (3.9)$$

Here  $A$  is the average brightness along the ellipse.

Notice that both techniques begin their series at  $j = 3$ ; terms with  $j < 3$  are not needed if the center, ellipticity, and position angle of the isophote have been fit correctly. The results obtained using these two methods are equivalent provided that departures from ellipticity are relatively small. Most published data use isophote fitting and parameterize the results in terms of the ratios  $a_j/a$  and  $b_j/a$ .

As a rule, the most significant non-elliptical term is the  $a_4$  coefficient, which is typically in the range  $-0.02 < a_4/a < 0.04$ . Galaxies with  $a_4 < 0$  are termed ‘boxy’ since their isophotes are somewhat rectangular, while those with  $a_4 > 0$  are accurately described as ‘pointed’, though the term ‘disky’ is widely used since many such galaxies appear to contain disks. An example is shown

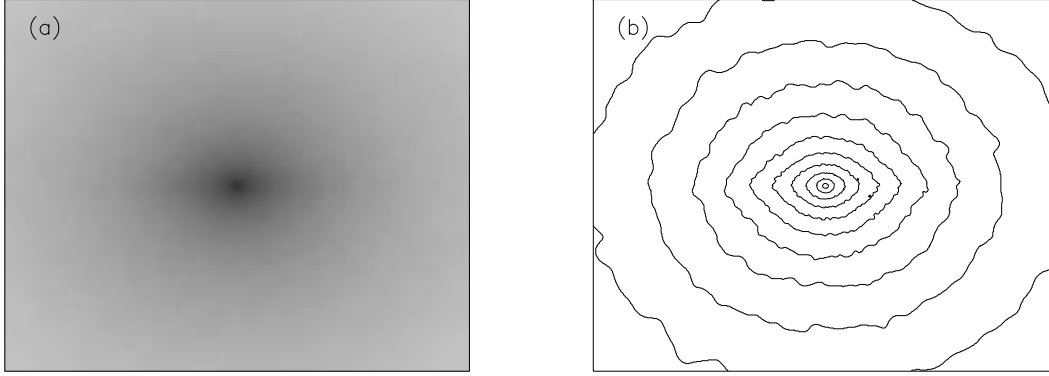


Figure 3.3: Model of an oblate E2 galaxy containing a disk. The spheroid has a luminosity profile  $j(r) \propto r^{-1}(1+r)^{-3}$ ; the disk has an exponential surface density profile  $\Sigma(r) \propto e^{-r}$ . Both components were scaled to have the same projected half-light radius when viewed face-on. The disk contains 12.5% of the total luminosity. In this view, the disk is  $15^\circ$  from edge-on. (a) Half-tone image. (b) Isophotes; note the “lemon-shaped” contours near the center.

in Fig. 3.3.

In a sample of 42 early-type galaxies, 10% had  $a_4/a > 0.02$  (Lauer 1985a) and thus seem likely to contain embedded disks. However, the actual percentage of ellipticals with embedded disks could be much larger. Photometric models combining a spheroidal  $r^{1/4}$  bulge and an exponential disk show that embedded disks must be either very substantial or nearly edge-on to be readily detected. Detection statistics are consistent with the hypothesis that *all* ellipticals with  $a_4 > 0$  contain disks contributing 20% of the total light (Rix & White 1990).

### 3.4 Radial Gradients

As a rule, E galaxies become *redder* toward their centers. These gradients are fairly subtle; a factor of 10 decrease in radius typically produces a change of  $\sim 0.25$  mag in  $(U - R)$  and  $\sim 0.1$  mag in  $(B - R)$  (Franx, Illingworth, & Heckman 1989b). Such gradients are fairly tricky to measure accurately since they are quite sensitive to sky background subtraction.

Two general explanations for such gradients have been discussed in the literature; the centers of galaxies may be older, or they may be more metal-rich. These possibilities may be distinguished by examining gradients of stellar absorption features in the integrated spectra of E galaxies. Hydrogen lines are characteristic of young stars; they become fainter as a stellar population ages. Conversely, lines of Mg and other elements are stronger in metal-rich populations.

A variety of observational results support the notion that color gradients are primarily due to radial gradients in metal abundance (Faber 1977). In particular, Mg and Fe lines become stronger with decreasing radius, while  $H\beta$  lines may either increase or decrease in strength (Gorgas & Efsthathiou 1987; Fisher, Franx, & Illingworth 1995). In some cases,  $H\beta$  absorption features may be filled in by line emission from diffuse gas. The observed gradients are consistent with metal abundances increasing by a factor of  $\sim 2$  over a factor of 10 decrease in radius (KD89; Fisher, Franx, & Illingworth 1995).

Spectral synthesis models indicate that the stars at any given radius span a range in metal abundance (e.g. Pickles 1987). This is consistent with the 2 dex spread in metallicity seen in the bulge of the Milky Way (Whitford & Rich 1983). Evidence for a spread in ages is seen in the deep Balmer lines of some systems and in indications of blue light above & beyond what one expects for a purely old population (Pickles 1987).

## 3.5 Shells & Fine Structures

The surface brightness of E galaxies doesn't always decline smoothly and monotonically with radius. When a smooth luminosity profile is subtracted from the actual surface brightness, 'shells' or 'ripples' may be seen (Malin & Carter 1980, Prieur 1990). At least 17% of field E galaxies have shell-like features, and the true fraction may be more than 44% (KD89).

Shells have spectral energy distributions characteristic of starlight. In many cases the shells are somewhat more blue than the galaxies they occupy (KD89). Shell systems have a variety of morphologies; some galaxies have shells transverse to the major axis and interleaved on opposite sides of the center of the galaxy, while other galaxies have shells distributed at all position angles (Prieur 1990). Both the colors and the varied morphologies of shells can be explained by accretion events in which a large elliptical galaxy captures and tidally disrupts a smaller companion.

Profile subtraction sometimes reveals other kinds of structures in E galaxies, including plumes, linear features or 'jets' (*not* the jets seen in AGNs!), 'X-structures', *etc.* (Schweizer & Seitzer 1992). Many of these features indicate dynamical disturbances which will eventually disappear as the stars comprising them pursue their individual orbits.

## 3.6 Interstellar Gas

### 3.6.1 Cold gas & dust

Many elliptical galaxies have dust lanes produced by cold interstellar material distributed in disks or rings (e.g. van Gorkom 1992). These flattened structures produce distinctive photometric signatures when seen nearly edge-on, as Fig. 3.4 shows. Velocity measurements show that in many cases the cold gas counter-rotates or is otherwise kinematically distinct from the underlying stellar component; a likely interpretation is that this material has been accreted since the galaxy formed.

Unlike stars, the gas can only settle down on closed (and stable) orbits. In theory this might allow determination of the principal planes of a galaxy's potential, but in practice settling times are long enough that this is questionable (KD89).

One galaxy in which a gas ring *does* define the principal plane is IC 2006 (Schweizer 1987; Franx, van Gorkom, & de Zeeuw 1994). This galaxy has an external ring containing some young stars. Neutral hydrogen observations show that the velocity varies along the ring in a remarkably sinusoidal manner, indicating that the ring - and the potential it moves in - is almost exactly circular. The inclination angle of the ring is  $37^\circ$ .

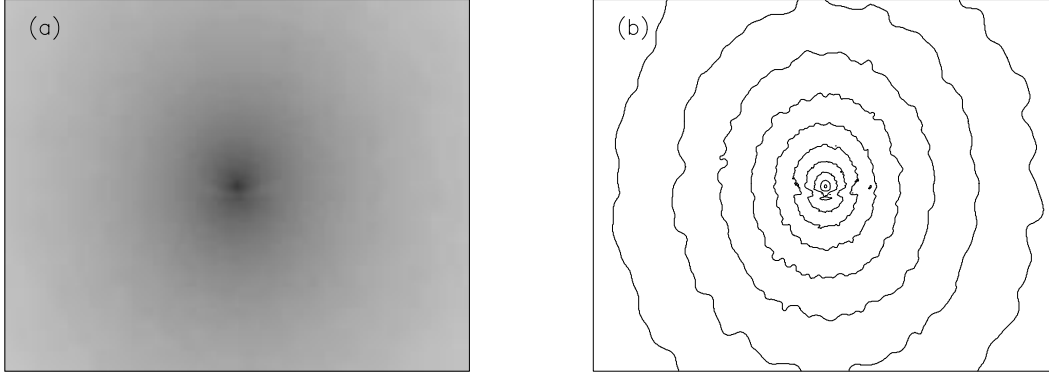


Figure 3.4: Model of a prolate E2 galaxy containing a dust ring. The spheroid has a luminosity profile  $j(r) \propto r^{-1}(1+r)^{-3}$ ; the ring has a surface density profile  $\Sigma(r) \propto r^{-1}$ . If viewed face-on, the ring would produce 0.25 magnitudes of extinction at its inner edge. In this view, the ring is  $15^\circ$  from edge-on. (a) Half-tone image. (b) Isophototes; note the “waist” created by the ring.

### 3.6.2 Hot gas

X-ray observations indicate that many ellipticals contain  $10^9$  to  $10^{10}$  solar masses of gas at temperatures of  $10^7$  K (Forman et al. 1979, Trinchieri & Fabbiano 1985, Schweizer 1987). This is comparable to the mass of cold and warm gas present in typical spiral galaxies; thus it seems fair to say that ellipticals are not, in fact, gas poor compared to disk galaxies. The hot gas typically forms a pressure-supported ‘atmosphere’ around the galaxy.

## 3.7 Globular Cluster Populations

On high-resolution images of nearby galaxies, globular clusters are evident as slightly extended objects. The number of globulars found in a galaxy is generally parameterized by the *specific frequency*,

$$S_N \equiv N_{GC} 10^{-0.4(M_V+15)} \quad (3.10)$$

where  $N_{GC}$  is the total number of globulars observed (corrected, if necessary, for incompleteness at faint levels) and  $M_V$  is the galaxy’s absolute magnitude. In effect,  $S_N$  is the number of globular clusters per unit galaxy luminosity, where unit luminosity corresponds to  $M_V = -15$ . Globulars are found in all kinds of galaxies, but it seems appropriate to discuss them here because they are much more common in E and S0 galaxies (see MB98, Fig. 4.63). Some ellipticals are staggeringly rich in globular clusters; for example, over 6000 have been identified in the giant elliptical M87, while a spiral galaxy like the Milky Way contains only a few hundred.

For nearby galaxies it’s possible to take a fairly complete census of globular clusters and thereby derive a cluster luminosity function. Absolute magnitudes of globular clusters appear to be drawn from a Gaussian distribution with a mean  $M_V$  of roughly  $-7.3$  and a dispersion of  $\sim 1.2$  magnitudes. This cluster luminosity function appears to be fairly universal in normal galaxies of various types; on the other hand, cluster populations in some interacting systems include a non-Gaussian “tail” to much larger luminosities (e.g. Schweizer 1996).

Globular clusters in the Milky Way exhibit a fairly narrow range of colors, consistent with old ( $\sim 12$  Gyr) populations of moderately metal-poor ( $[\text{Fe}/\text{H}] \sim -1.5_{-0.5}^{+1}$ ) stars. In M87, on the other hand, we find a bimodal color distribution with one peak matching the Milky Way's and another which is even redder. These red colors are presumably due to higher metallicity rather than more extreme age, but M87's globulars are too faint for effective spectroscopy. In the nearby peculiar elliptical NGC 5128 (Cen. A) the globulars are bright enough for spectroscopic analysis; the results show a bimodal metallicity distribution, with metal-poor *and* metal-rich components (Held et al. 1997; Peng, Ford, & Freeman 2004a).

### 3.8 Stellar Kinematics

Spectra of elliptical galaxies exhibit absorption features similar to those seen in the late-type giant stars which dominate the light from old stellar populations, but these features are shifted and broadened as a result of stellar motions. By convolving the spectrum of an appropriate template star with a Gaussian it is often possible to match the observed spectrum of a galaxy (e.g. BM98, Fig. 11.4). The mean of the Gaussian yields the mean stellar line-of-sight velocity, while the dispersion of the Gaussian yields information on the spread of stellar velocities.

By placing the spectroscope slit along the major axis one can measure the mean velocity  $V$  and velocity dispersion  $\sigma$  as functions of major-axis position. Velocity dispersions usually peak at the centers of galaxies and fall off on either side of the center. Relative to systemic velocity, mean velocities generally exhibit opposite signs on opposite sides of the center, indicating some amount of rotation. It is almost immediately evident, however, that rotation velocity is *not* correlated with observed ellipticity in bright ellipticals. For example, NGC 2663, NGC 3706, and NGC 5018 are all E3 galaxies, yet rotate with very different velocities (see BM98, Fig. 11.6).

If elliptical galaxies were oblate configurations rotating about their short axes, a spectra taken with the slit placed along the projected minor axis should yield  $V$  equal to systemic velocity independent of position. In fact, many ellipticals exhibit minor-axis rotation; more generally, the apparent rotation axis and the apparent minor axis may be misaligned (Franx et al. 1991; BM98, Fig. 11.10). While in most galaxies these misalignments are modest, a few galaxies appear to rotate primarily about their minor axes.

In most cases, measurements of integrated spectra are limited by surface brightness to about one effective radius or less from the center. To probe the kinematics at larger radii we can use planetary nebulae. These nebulae emit most of their light in a few spectral lines, so they can easily be identified by comparing a broad-band image with one taken using a narrow-band filter. Line-of-sight velocities for individual nebulae may be determined by fiber spectroscopy (e.g. Ciardullo, Jacoby, & Dejonghe 1993; Hui et al. 1995) or slitless spectroscopy (Mendez et al. 2001). In NGC 5128, planetary nebulae have been detected out to  $\sim 80$  kpc from the center of the galaxy; the velocity field revealed by these nebulae shows a dramatic twist in the systemic velocity contour, which is close to the optical minor axis at small radii but nearly aligned with the major axis at large radii (Peng, Ford, & Freeman 2004b).

The inner regions of elliptical galaxies often exhibit unusual kinematics; for example, about a quarter of all elliptical galaxies have inner regions which *counterrotate* or are otherwise “kinematically decoupled” from their parent galaxies (KD89). These decoupled central regions seem to

contain distinct stellar populations with high metallicity (Bender & Surma 1992). High-resolution color maps of kinematically decoupled centers often show unusual features including disks or rings of dusty gas (Carollo et al. 1997).

### 3.8.1 Velocity profiles

More information may be extracted from galactic absorption-line spectra by relaxing the assumption that the line-of-sight velocity distribution is a Gaussian. Such an analysis may be performed in several different ways (Rix & White 1992):

- **Fourier transform methods** invoke the convolution theorem; the transform of the observed spectrum is (approximately) equal to the transform of the velocity profile times the transform of the template spectrum (Sargent et al. 1977; Franx, Illingworth, & Heckman 1989a).
- **Cross-correlation methods** measure the correlation between the observed and template spectra as a function of the relative shift in wavelength (Tonry & Davis 1979, Bender 1990).
- **Direct methods** synthesize the observed spectrum by adding up shifted versions of the template spectrum. This is somewhat expensive computationally but avoids the ‘belling’ needed to produce well-behaved transforms of finite spectral intervals, allows masking of discrepant features to reduce mismatch between template and galactic spectra, and permits a straightforward error analysis (Rix & White 1992).

Non-Gaussian line profiles are often characterized using the Gauss-Hermite series (van der Marel & Franx 1993):

$$LP(v) = \Gamma \frac{\alpha(w)}{\sigma} \sum_{j=0} h_j H_j(w), \quad w = \frac{v-V}{\sigma}, \quad (3.11)$$

where  $\Gamma$  is the line strength,  $\sigma$  is the velocity dispersion,  $V$  is the mean velocity, and

$$\alpha(x) = (2\pi)^{-1/2} \exp(-x^2/2) \quad (3.12)$$

is a normalized Gaussian with unit dispersion. The set of functions  $H_j(x)$  are *Hermite polynomials* of degree  $j$ ; these are orthogonal with respect to the weight function  $\alpha(x)^2$ :

$$2\pi^{1/2} \int dx H_j(x) H_k(x) \alpha(x)^2 = \delta_{jk}. \quad (3.13)$$

In applying (3.11), the parameters  $\Gamma$ ,  $\sigma$ , and  $V$  are chosen by requiring that  $h_0 = 1$  and  $h_1 = h_2 = 0$ ; non-Gaussian line profiles yield nonzero  $h_j$  for  $j > 2$ . In particular,  $h_3$  parametrizes the skewness of the line profile, while  $h_4$  measures whether the profile is more or less peaked than a Gaussian.

### 3.8.2 Embedded disks

Photometric analysis is often unreliable in detecting embedded disks and recovering disk parameters. The practice of finding the best-fit ellipse and attributing only the residuals to the disk *systematically* underestimates the luminosity contributed by the latter (Rix & White 1990). Moreover, surface-brightness data cannot unambiguously detect disks unless they are fairly close to edge-on.

Line-of-sight velocity profiles provide a more definitive diagnosis. Profiles characteristic of embedded stellar disks are found in many elliptical galaxies (Franx & Illingworth 1988, Bender

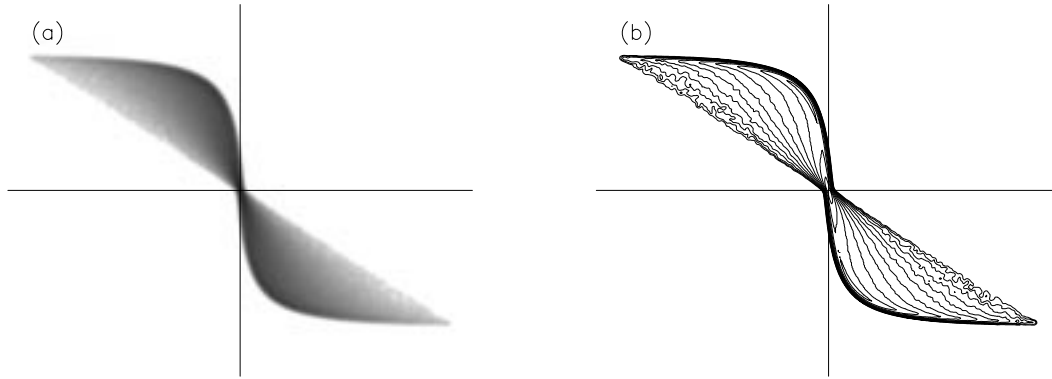


Figure 3.5: Line-of-sight velocity distribution for an exponential disk viewed edge-on.

1990a, Rix & White 1990, 1992, van der Marel & Franx 1993, van der Marel et al. 1994a). As Fig. 3.5 shows, a disk seen edge-on produces distinctly asymmetric line profiles; in terms of the Gauss-Hermite parameterization, such profiles have  $V$  and  $h_3$  of *opposite* signs. The characteristics of these embedded disks show considerable variation: NGC 5322 has a relatively ‘warm’ disk, with  $v/\sigma = 1.4$ , while the disk in NGC 3610 is quite ‘cold’, with  $v/\sigma = 4.5$  (Rix & White 1992).

Isophote shape is known to be correlated with rotation velocity: Elliptical galaxies with  $a_4 > 0$  tend to be rapid rotators (Bender 1988; KD89). Kinematically cold disks may be partly responsible for this correlation, since at some radii such disks can make substantial contributions to the light and tend to dominate line-of-sight velocity measurements parametrized by simple Gaussians (Rix & White 1990). For example, purely Gaussian fits to composite line profiles may overestimate rotation curve amplitudes by  $> 30\%$  (van der Marel & Franx 1993).

### 3.9 Parameter Correlations

Elliptical galaxies exhibit a bewildering variety of correlations. However, one set of three correlations seems to tell a consistent story:

- The integrated colors of E galaxies show systematic trends with luminosity; brighter galaxies are redder by  $\sim 0.1$  mag in  $(u - V)$  per 1 mag increase in  $L$  (MB81, Chap. 5-4).
- The luminosities of E galaxies are highly correlated with their velocity dispersions; this is generally expressed as a power law,

$$L \propto \sigma^n, \quad (3.14)$$

where  $L$  is the galaxy luminosity,  $\sigma$  is the central line-of-sight velocity dispersion, and the index  $n$  is about 4 (Faber & Jackson 1976; KD89).

- Velocity dispersion is correlated with metal abundance; galaxies with large  $\sigma$  are more metal rich (Faber 1973; Bender, Burstein, & Faber 1993).

These trends can be understood if the colors of E galaxies are governed by their metallicity. In this interpretation, galaxies with high  $\sigma$  have deeper potential wells, and are therefore more likely to retain metals produced by supernovae. According to (3.14), such galaxies also have higher luminosities.

Finally, the higher metal abundances of these galaxies increase the amount of UV line-blanketing and therefore lead to redder colors as observed.

A significant correlation is also seen between the effective (or half-light) radius,  $R_e$ , and the surface brightness at that radius,  $I_e$ :

$$R_e \propto I_e^{-0.83} \quad (3.15)$$

(KD89). This implies that luminous galaxies have lower average surface brightnesses.

### 3.9.1 Central parameter correlations

High-resolution surface photometry shows some elliptical galaxies have breaks (once known as ‘cores’) where their luminosity profile slopes change decrease markedly, while other ellipticals show a constant or only gradually changing slope to the innermost point measured. Direct imaging (Kormendy et al. 1994) and nonparametric deprojection of luminosity profiles (Gebhardt et al. 1996) both dramatize the difference between resolved breaks and power-law profiles. But parameter correlations offer some support to the possibility that some power-law profiles actually break at projected radii smaller than 0.1 arcsec.

Perhaps most basic is the roughly linear correlation between absolute spheroid luminosity and physical break radius (Kormendy et al. 1994, Faber et al. 1997). Many of the power-law profiles belong to galaxies fainter than  $M_V = -21$ ; some of these galaxies could well have breaks at radii  $R_b < 10$  pc and may follow the correlation found for the well-resolved galaxies. On the other hand, there are moderately luminous galaxies with upper limits on  $R_b$  well below the mean trend for galaxies with well-resolved breaks. Luminosity also correlates with central velocity dispersion  $\sigma_0$  and with surface brightness  $I_b$  at radius  $R_b$ .

### 3.9.2 Two kinds of E galaxies?

Kormendy & Bender (1996) have proposed that boxyness or diskyness be adopted as the primary classification criterion for elliptical galaxies. Isophotal shape correlates with several other important characteristics (e.g. Bender 1990b), so this proposal manages to organize a large number of observed correlations into one coherent picture as outlined in Table 3.1.

	<b>Boxy</b> ( $a_4 < 0$ )	<b>Disky</b> ( $a_4 > 0$ )
Luminosity	high	low
Profile	break	power-law
Shape	triaxial	almost oblate
Flattening	anisotropy	rotation
Radio	loud	quiet
X-ray	loud	quiet

Table 3.1: The boxy-disky dichotomy for elliptical galaxies.

### 3.9.3 The fundamental plane

Most of the scatter in the Faber-Jackson relationship is *intrinsic*; it reflects real galaxy properties, not measurement errors. A number of authors attempted to identify the “second parameter” which would account for this scatter.

Modern data show that elliptical galaxies obey a relationship of the form

$$R_e \propto \sigma^{1.4} I_e^{-0.9} \quad (3.16)$$

(KD89). This is called *the fundamental plane* because in a space whose axes are  $\log R_r$ ,  $\log \sigma$ , and  $\log I_e$ , elliptical galaxies lie on a rather thin, nearly planar surface. Note that the power-law index of  $I_e$  is nearly the same as in (3.15).

On dimensional grounds, a self-gravitating system should obey a relationship of the form

$$\sigma^2 \propto G \frac{M}{R} \quad (3.17)$$

where  $G$  is the gravitational constant,  $M$  is a characteristic mass, and  $R$  is *e.g.* the half-mass radius. In terms of the system’s mass-to-light ratio ( $M/L$ ), this implies

$$R \propto \sigma^2 I_e^{-1} (M/L)^{-1}, \quad (3.18)$$

a relationship very similar to (3.16).

The fact that the exponents of  $\sigma$  and  $I_e$  appearing in (3.18) are not quite the same as those in (3.16) can be explained if  $(M/L)$  is a slowly-varying function of galaxy mass (KD89); the observed exponents are consistent with (3.18) if

$$(M/L) \propto M^{0.2}. \quad (3.19)$$

The fundamental plane is a valuable tool for estimating distances to galaxies;  $\sigma$  and  $I_e$  are measured from spectroscopy and photometry and used in (3.16) to obtain the physical radius  $R_e$  in kpc; comparison with the apparent  $R_e$  then yields the distance. But if  $(M/L)$  is a function of galaxy environment, then this procedure will yield biased estimates of the distance. Some researchers have found evidence that the fundamental plane does depend on cluster richness (KD89).

### 3.9.4 Core fundamental plane

In galaxies with well-resolved central breaks the parameters obey a ‘fundamental plane’ relationship involving  $R_b$ ,  $I_b$ , and  $\sigma$  (Faber et al. 1997). This plane is analogous to one the described above for  $R_e$ ,  $I_e$ , and  $\sigma$ . The existence of such a plane may imply that the virial theorem rules the parameters at the break radius; however the central plane seems thicker than the global plane, hinting that central  $M/L$  ratios vary from galaxy to galaxy.

## Problems

**3.1.** Suppose that **all** elliptical galaxies have embedded stellar disks, but that these disks can only be seen when viewed within  $\pm 15^\circ$  of edge-on. Assuming that elliptical galaxies are randomly oriented in space, calculate the fraction which will exhibit visible disks.

**3.2.** As discussed in § 3.3.1 above, non-elliptical isophote shapes may be described by the expansion (3.8) of  $\delta R(\theta)$  in trigonometric functions (see Fig. 4.20 of BM98). Sketch an ellipse with an axial ratio of 0.6; next, separately sketch the non-elliptical isophotes which result if (a)  $a_3 > 0$ , (b)  $b_3 > 0$ , (c)  $a_4 > 0$ , and (d)  $b_4 > 0$ .

**3.3.** Consider a disk with a power-law surface density profile  $\Sigma(r) \propto r^{-2}$ ; let the disk rotate with a circular velocity  $v_c$  which is independent of  $r$ . Suppose you observe this disk edge-on along a sight line which is offset from the center of the disk. Let  $F(v)dv$  be the number of stars with line-of-sight velocities in the range  $v$  to  $v + dv$ . Calculate the functional form of  $F(v)$  (without worrying about the overall normalization). (Hints: #1 if you find yourself doing an integral, you're probably on the wrong track; #2 see BM98, Problem 11.6.)